

Highlighting research from the Liquid Crystal Institute and the Department of Biological Sciences at Kent State University, from the group of Dr Elda Hegmann.

Liquid crystal elastomer foams with elastic properties specifically engineered as biodegradable brain tissue scaffolds

Liquid Crystal Elastomers (LCEs) have been long sought as artificial tissues based on a combination of orientational ordering, induced by liquid crystalline moieties, and elastic properties of polymers. Here we show a platform that provides a new insight into LCE–cell interactions where liquid crystalline materials promote cell alignment for appropriately stimulated tissue regeneration.

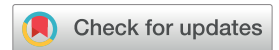




Soft Matter



PAPER



Cite this: Soft Matter, 2018, **14**, 354

Received 29th September 2017, Accepted 5th December 2017

DOI: 10.1039/c7sm01949a

rsc.li/soft-matter-journal

Liquid crystal elastomer foams with elastic properties specifically engineered as biodegradable brain tissue scaffolds†

M. E. Prévôt, Dab H. Andro, S. L. M. Alexander, S. Ustunel, Dabd C. Zhu, De Z. Nikolov, f S. T. Rafferty, M. T. Brannum, B. Kinsel, a L. T. J. Korley, bc E. J. Freeman, J. A. McDonough, R. J. Clements* and E. Hegmann **D** **abd

Tissue regeneration requires 3-dimensional (3D) smart materials as scaffolds to promote transport of nutrients. To mimic mechanical properties of extracellular matrices, biocompatible polymers have been widely studied and a diverse range of 3D scaffolds have been produced. We propose the use of responsive polymeric materials to create dynamic substrates for cell culture, which goes beyond designing only a physical static 3D scaffold. Here, we demonstrated that lactone- and lactide-based star block-copolymers (SBCs), where a liquid crystal (LC) moiety has been attached as a side-group, can be crosslinked to obtain Liquid Crystal Elastomers (LCEs) with a porous architecture using a salt-leaching method to promote cell infiltration. The obtained SmA LCE-based fully interconnected-porous foams exhibit a Young modulus of 0.23 \pm 0.07 MPa and a biodegradability rate of around 20% after 15 weeks both of which are optimized to mimic native environments. We present cell culture results showing growth and proliferation of neurons on the scaffold after four weeks. This research provides a new platform to analyse LCE scaffold-cell interactions where the presence of liquid crystal moieties promotes cell alignment paving the way for a stimulated brain-like tissue.

Introduction

The story of liquid crystalline materials as artificial muscles begins with O. Lehmann's discovery. In 1909, he suggested the construction of an artificial muscular driving motor using molecular forces within a liquid crystal phase ("...Mais le but principal est l'application des nouveaux phénomènes découverts, par example, l'emploi des forces moléculaires pour la construction d'un moteur musculaire artificiel,..."). A semi-fast artificial

muscle was then conceived by de Gennes, in 1997, based on a nematic liquid crystal elastomer (LCE).2 LCEs are characterized by their orientational ordering derived from their liquid crystalline units combined with the rubbery elasticity properties of a polymer network. Over the past decade, LCEs have been widely used as smart materials for biological applications. For example, Li et al. have created a thermo-responsive contraction material built from a network of side-on nematic LC homopolymers.³ Sánchez-Ferrer et al. have developed a microvalve in which the actuation process is given by the thermo-expansion and shrinkage of an LCE according to the direction of the director.4 In 2016, Agrawal et al. showed that LCEs could be used as dynamic substrates for culturing cells during electrical stimulation.⁵ Within this field of study, our research area focuses on creating a better approach to typical cell culture models being hampered by their two-dimensional nature (cell suspension), with externally stimulated liquid crystal units to promote cell alignment under LCE deformation.

Tissue engineering involves the formation of functional substitutes for the therapeutic reconstruction of (damaged) tissue. This is made by the stimulation of selected target cells through a systematic combination of molecular and mechanical signals,⁷ and appropriate scaffold materials that provide support as well as 3D growth and proliferation. Scaffold materials must provide

^a Liquid Crystal Institute, Kent State University, 1425 Lester Lefton Esplanade, Kent, OH 44242, USA

^b Department of Biological Sciences, Kent State University, 850 Lester Lefton Esplanade, Kent, OH 44242, USA. E-mail: rclement@kent.edu, ehegmann@kent.edu

^c Macromolecular Sciences and Engineering Department, Case Western Reserve University, 2100 Adelbert Road, Cleveland, OH 44106, USA

^d Chemical Physics Interdisciplinary Program, Kent State University, 1425 Lester Lefton Esplanade, Kent, OH 44242, USA

^e Advanced Light Source, Lawrence Berkeley National Laboratory, 1 Cyclotron Road, Berkeley, CA 94720, USA

 $[^]f$ National Polymer Innovation Center, College of Polymer Science and Polymer Engineering, The University of Akron, 240 S Forge Street, Akron, OH 44325, USA † Electronic supplementary information (ESI) available: LCE synthesis and characterization data, thermal analysis, SEM, and confocal microscopy images. See DOI: 10.1039/c7sm01949a

specific properties to create an appropriate cell environment for the development of cells and extracellular matrix. Thus, an ideal 3D scaffold should satisfy specific requirements: (i) be biocompatible,8 (ii) exhibit mechanical properties mimicking native environments; (iii) have a porous well interconnected architecture, 9-12 and (iv) biodegrade at a rate that matches the regeneration of new tissue (taking into account ECM formation) and into non-toxic products that can easily be resorbed or excreted first by the cells, and finally by the body. 13

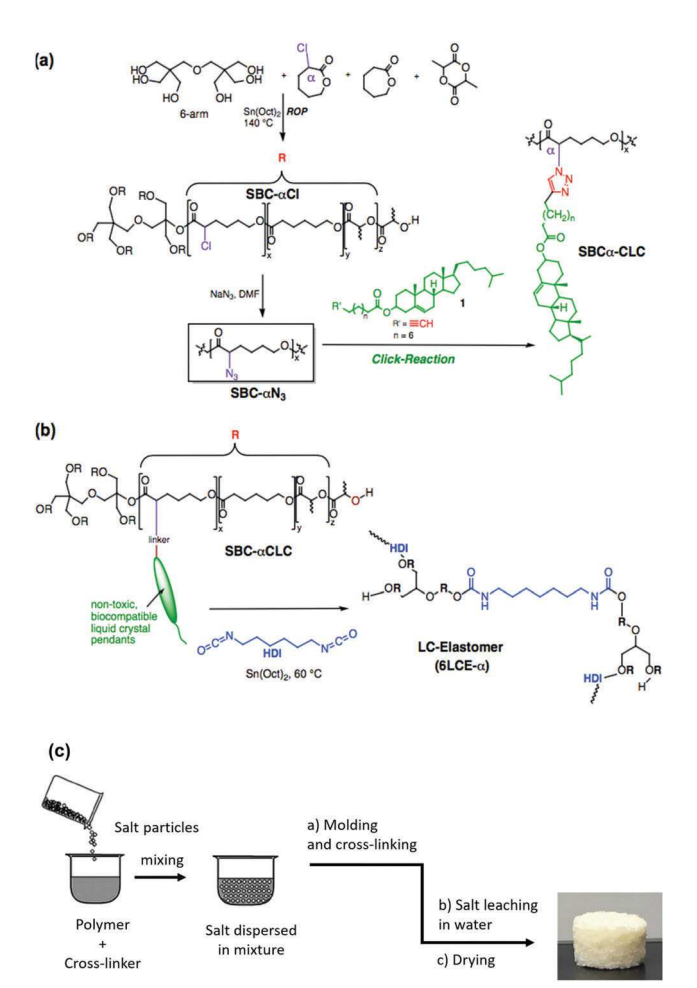
A wide variety of 3D-scaffolds have been studied by the scientific community, such as hydrogel-based, 14-20 fibrous, 21,22 microsphere, 23,24 and polymeric scaffolds. Mostly because hydrogels can be formulated from diverse types of polymers with tunable mechanical properties they are used as materials to support neuronal tissues. Here, we propose to overcome the lack of porosity or pore size distribution usually found in hydrogels by using 3D polymeric porous scaffolds where we can specifically incorporate any pore size or shape. The typical scaffold design includes sponge or foam morphologies, by using a template or a specific leaching method.²⁵ Particle leaching methods consist of creating porous structures from a hardened polymer and leaching particles. Typically leaching particles are dissolved in a solvent (typically water or alcohol), to wash them out after the cross-linking process. Salt crystal size is carefully selected to obtain a particular pore size to match the cells of interest. Then, the salt crystals are dispersed in a solution containing the polymer mixture and the crosslinker; the polymer solution penetrates into the spaces created by the salt particles. The resulting mixture is then molded, heated, and finally washed to remove the salt particles. A solid sponge-like material is obtained where the foam's air area forms the pores of the final scaffold. The original shape of the salt particles governs the pore shape of the 3D LCE. This method can utilize a leachable particle with easily designable shape and size to provide a tunable 3D morphology for the design of various tissues. In this setting, sodium chloride (NaCl) appears adequate, as its shape and size have been proven to be modulated using several methods.²⁵ In addition, salt is characterized by its low cost, and its intrinsic capability to dissolve in water.²⁶

The aim of this study is to create 3D porous LCE foams as host scaffold for brain cells with the capability to become a stimulated substrate. Neurons and glial cells are major cell types of the central nervous system. The viability and expansion of cells is governed by constitutive parameters of the scaffold, such as porosity²⁷ as well as stiffness of the substrate to which the cells are adhered, 28 and these parameters need to be carefully controlled.

Synthesis and morphology of LCE foam

Synthesis and chemical characterization of polymers preparation of LCEs

Scheme 1 shows the synthetic pathway followed for the preparation of LCEs based on our earlier work. As reported previously, the mechanism is based on a random ring opening



Scheme 1 Synthesis pathways of a star block-copolymer with cholesterol liquid crystal pendants: (a) 6SBC- α CLC. The ratio of all caprolactones to D,L-lactide is 1:1; the ratio between chlorine-modified and non-modified caprolactone is 1:10, (b) 6LCE- α . The ratio between 6SBC- α CLC and the cross-linker is 1:40, and (c) the foam preparation procedure.

polymerization of dipentaerythritol as the 6-arm initiator, ε-caprolactone (ε-CL), modified ε-caprolactone (α-chloro-εcaprolactone (α-Cl-ε-CL)), and (D,L)-lactide (D,L-LA) (Scheme 1a). ^{29–32} In this reaction, tin(II) 2-ethylhexanoate is used as a catalyst to obtain a 6-arm star block-copolymer (6SBC-αCl). Substitution of the halogen atom (-Cl) by an azide group (-N₃), named as 6SBC-αN₃, allows a modified cholesterol (LC) to be covalently attached as a pendant to the polymer backbone using a 5-membered ring via an alkyne-azide Huisgen's cycloaddition reaction ("click" reaction). Cholesterylhexynoate is chosen as the LC unit, due to its cholesterol-based nature conferring biocompatibility. 6SBC-αCLC was characterized by proton Nuclear Magnetic Resonance (1H NMR) and Fourier-Transform Infra Red spectroscopy (FT-IR).

The synthetic transformations are followed by ATR (attenuated total reflection) FT-IR spectroscopy, i.e. by the appearance of the 2100 cm⁻¹ band corresponding to the displacement of the chloro by an azide group. This substitution is further confirmed by ¹H NMR spectroscopy considering the higher chemical shift of the proton bound to the same carbon atom as the azide-group.

The attachment of the LC pendant to the SBC was confirmed by FT-IR, *i.e.* by the disappearance of the 2100 cm $^{-1}$ band and the appearance of a new band at 3260 cm⁻¹ corresponding to the presence of a triazole ring. The formation of the triazole ring was also indicated by the presence of a singlet observed at 7.31 ppm in ¹H NMR spectra. Hexamethylene diisocyanate (HDI) was chosen as the crosslinker (forming urethanes) because of its low processing temperature and its frequent use as a crosslinker in polymer scaffolds used in tissue engineering (Scheme 1b).33 For synthetic details, see the ESI.†

Porous 3D morphology

A salt leaching method is used in this study to create a 3D porous scaffold, which promotes neuronal tissue growth. This method consists in mixing 6LCE- α , solvent (ϵ -CL), crosslinker and salt in a ratio of 4:2:1:160 and pouring the obtained mixture into a mold. Mechanical compression is used to assure the integrity of the foam and increase the pore interconnectivity of the porous scaffold.²⁵ After crosslinking with HDI, the SBC (6SBC- α CLC) becomes the 6LCE- α foam. The salt is then removed by leaving the foam in water for 3 days followed by drying the foam in air (Scheme 1c).

Using a 3D-scaffold for cell culture studies allows for an optimized internal morphology, namely porosity and pore size. The size of neuroblastoma SH-SY5Y cells is known to be approximately 10 to 25 $\mu m.$ Thus, for elastomer seeding, a minimum 25 µm pore size foam is essential. However, we already considered that if co-culturing with other cells is required, including their diffusion inside the porous scaffold, larger pores might be needed. To promote vascularization, as insufficient vascularization is synonymous with cell death in tissue-engineered constructs, the final morphology was designed to have enough space for cell growth and proliferation, 35 as well as to facilitate nutrient and oxygen diffusion as well as waste removal.¹⁹ The ideal morphology for tissue engineering is to obtain a scaffold with large and high-density pores. In the current study, a high surface area-to-volume ratio for the interconnected porous scaffolds was directly correlated with the amount and leaching of commercially available salt crystals with an average size of 180 µm.

We used two methods to calculate the porosity of the materials. On both methods, the total porosity is calculated as the volume of all pores (open and closed pores) as a percentage of the total of the solid LCE plus pore (open and closed) volumes within the volume of interest (VOI). During the process of porosity determination a VOI having ideal cylindrical shape in the middle of the sample was defined for the calculations in such a way that all the peripheral regions and the boundaries of the sample with air were not included in the analysis.

First, a 3D confocal microscopy reconstruction of the obtained LCE foam allowed for a direct observation of the internal morphology of the foam (Fig. 1). The final 6LCE foams are characterized by highly interconnected pores, and exhibit 84% porosity.

The second method used to corroborate our porosity findings was using a Micro CT Scanner. The samples of LCE foam were

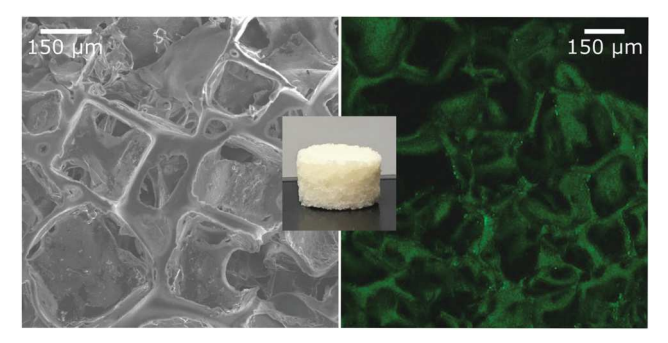


Fig. 1 Left; SEM image, and right; confocal micrograph showing the internal morphology of 6LCE-α foam. Inset: Image of disk-molded LCE foam.

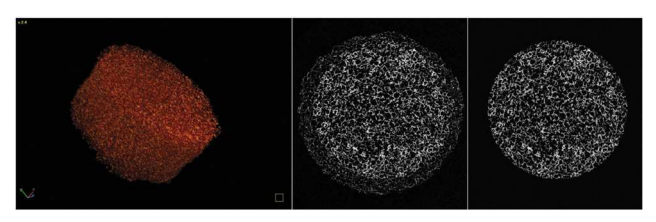


Fig. 2 Far left: Micro CT 3D volume rendering of an LCE sample. Middle and right: Reconstructed image of a 2D layer of LCE foam sample showing selection of a circular Region of Interest (ROI) to define the VOI with a cylindrical shape for porosity analysis.

scanned using a SkyScan 1172 Micro CT Scanner (Bruker) where volume rendering of the 3D image of one of the samples is shown in Fig. 2. An appropriate grey level threshold was selected to define only the material of the sample while eliminating certain noise voxels (speckles) arising from the reconstruction algorithm. The porosity measured in this way is truly representative of the material under study.

The pore analysis provides information about the total number of closed pores, and volume of closed pores and open pores. An 'open pore' or 'broken pore' is a pore intersecting the boundary of the VOI, or in other words a pore that is connected to the outside in 2D or 3D. A 'closed pore' is a pore that is not connected to the outside in 2D or 3D and can be described as a group of black voxels that is fully surrounded by a border of white voxels. Black in our analysis is describing close to 100% transmission for the scanning X-ray beam. Open and closed porosity is measured after the total VOI is calculated.

The percentage of closed porosity of our samples is negligible (ca. 6×10^{-4} %). This is proof that all our pores are interconnected and have outlets to the outside of the VOI.

The total porosity of our samples was determined to be 77 \pm 5%, which is within the boundaries of the porosity value found by the confocal microscopy method.

Porosity of the material could be adjusted by varying the polymer mixture to salt ratio during preparation. In the future, this versatility will allow us to optimize the density of the scaffolds to favor size-specific cell infiltration. In this case, the pore size and density were optimized for brain cells, and can be easily adjusted to other cell types and sizes. We have

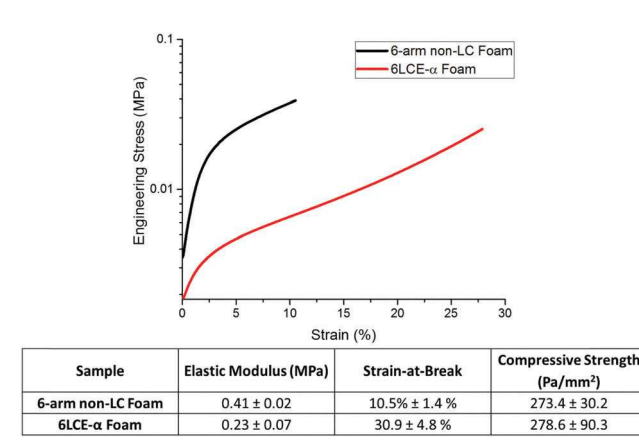


Fig. 3 Comparison of non-LC elastomer and 6LCE foam under compressive force.

found that the morphology of the 6LCE foams constitutes an appropriate prototype for brain cell growth.

Mechanical properties

The elasticity of brain tissue varies substantially in deeper regions of the brain and varies by brain area depending on cell type, structure, and vascularity. Dynamic mechanical analysis was utilized to explore the elastic properties of 6LCE- α foam. For comparison, a non-LC foam (6-arm non-LC foam) was synthesized following the synthetic path in Scheme 1, with the exception that there is no LC moiety as a pendant group. The 6-arm non-LC foam exhibited a slightly higher elastic modulus compared to the LCE foams (Fig. 3); however, a 20% increase in strain-at-break was observed for the 6LCE- α foams. The compressive strengths of the unmodified 6LCE- α foams were comparable due to similarities in porosity and network structure for the non-LC and LCE foams. Overall, the extensibility and modulus values of the 6LCE-α foams fall within the acceptable limits for investigating the proliferation of brain cells. Specifically, the elastic modulus is comparable in order of magnitude to those of spinal cord and gray matter tissues, ^{28,36} and compressive strains exceeding 30% are non-ideal due to resulting tissue damage.³⁷ Preliminary foam recovery experiments indicate that, qualitatively, the LCE foams are able to recover after deformation; quantitative experiments on foam recovery are ongoing.

Results and discussion

Liquid crystalline properties and thermal behavior

The liquid crystal properties were investigated using polarized optical microscopy (POM), differential scanning calorimetry (DSC), and small angle X-ray scattering (SAXS). The SAXS patterns show two sharp scattering peaks in the mid-angle region ($q_1 \approx 0.16 \text{ Å}^{-1}$ and $q_2 \approx 0.32 \text{ Å}^{-1}$) characteristic of a smectic phase (Fig. 4a). Additional peaks at 0.22 Å⁻¹ and $0.32~\mbox{Å}^{-1}$ are attributed to the reference signal (Kapton). The SAXS pattern obtained for the LCE foam matches with the results we reported previously.²⁹ Thus, in analogy, we assume a

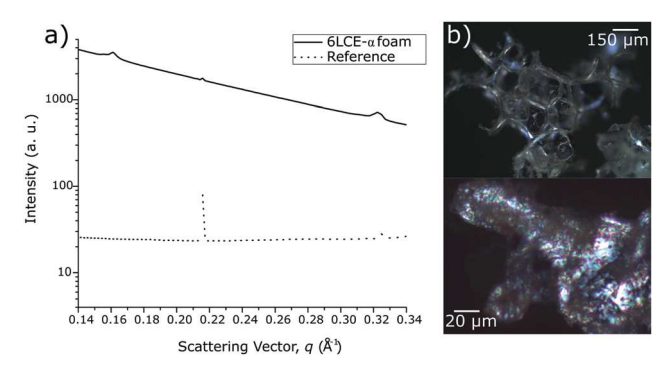


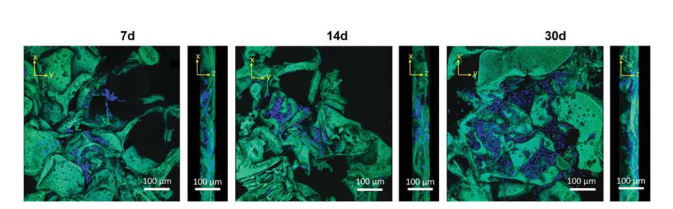
Fig. 4 (a) SAXS of $6LCE-\alpha$ foam taken at room temperature showing a pattern indicative of an SmA phase, and (b) POM micrographs of the 6LCE- α foam at room temperature (25 °C).

smectic-A (SmA) phase type ordering with interdigitated cholesterol moieties. POM observations of the LCE foam between two plain untreated glass slides show birefringent behavior (Fig. 4b). By gently applying pressure to the foam, some patterns similar to fan-textures appeared that corroborated the SAXS measurements, i.e. the formation of an SmA phase.

The thermal behavior was further probed by differential scanning calorimetry (DSC) and thermogravimetric analysis (TGA). DSC (Fig. S1, ESI†) allowed us to detect a clear glass transition at -60 °C using a heating and cooling rate of 10 °C min⁻¹ during two heating/cooling cycles. TGA (Fig. S2, ESI†), showed that the LCE samples are thermally stable up to 200 °C (only 1.7% weight loss at 200 °C). All of these values perfectly fit with our previously reported findings.^{29,30} Using POM, we recorded a phase transition from the isotropic liquid state to the SmA phase at 74 °C for 6SBC-αCLC indicating that the SmA phase is stable at and well below room temperature. This significant phase stability (>100 °C) makes them particularly suitable as dynamic substrates over a wide temperature range, but particularly at physiological temperature.

Cell affinity

To determine the viability of cells within the 6LCE foam, we evaluated SH-SY5Y cells as a first model of brain cells. The nuclei of SH-SY5Y cells have been stained blue using DAPI for better observation of cell infiltration within the LCE and cell anisotropy has been observed by identifying nuclei elongation. Fig. 5 shows the fluorescence confocal microscopy images of the LC foam (green) taken between two cover slips, illustrating cells cultured (blue) for 7, 14 and 30 days. After 7 days, cells attached to the elastomer indicating that the LCE platform



Confocal images (x, y- and x, z-plane) obtained in LCE foams (green) after 7 days (left), 14 days (middle), and 30 days (right) showing cell proliferation.

supports neuronal growth. After 14 days, cell number had increased (1.5-fold) compared to the number of cells observed at the first week time point. At 30 days cells continue growing (cell number increased 3.5-fold compared to week 1) and expanding throughout the LCE matrix. This is in agreement with previous cell viability data obtained from LCE scaffolds featuring identical chemical building blocks.³⁰ Furthermore, cells are observed growing on top and especially within the elastomer voids throughout its depth (see the ESI,† Fig. S7 for a 3D reconstruction), indicating that the open architecture allows infiltration of cells into deeper regions of the foam. In order to support long term cultures and in vitro development of cellular networks that consist of multiple layers, these neural scaffolds provide mechanisms to mechanically as well as spatially support distributed maturation of neurons while also ensuring access to media by promoting mass transport including waste removal. These initial results indicate that LCE foams show great promise as a platform to support the growth of three-dimensional neural networks for in vitro experimentation and bioengineering applications.

Degradation properties

Given the biocompatibility of the cholesterol pendants, we need to focus particularly on the biodegradability of the polymer backbone. The degradation of the \(\epsilon\)-caprolactone-D,L-lactide polymer backbone, composed of ester linkages, involves an auto-catalytic hydrolysis, known to produce non-toxic six-carbon fragments, 13 but also an enzymatic action. In this degradation study, we focused on hydrolysis degradation, without enzymatic considerations, and the foam tested contained no cells.

The brain has a high water content, about 80% water, which would imply fast hydrolytic degradation.³⁸ All specimens were also tested in water, a neutral buffer (PBS), and finally ethanol commonly used to sterilize elastomer foams. The measure of degradation is based on the loss of the foam's weight with time. First, swelling is observed in the foam with both water and PBS. This trend is followed by a slow and gradual loss of weight (20% degradation) over 15 weeks (Fig. 6).

At the end of week 15, none of the LCE foams had degraded completely, indicating that theoretically cell growth and the development of ECM will be ensured for long periods of time. To estimate optimal degradation time, different parameters such as the number of cells need to be considered. However, in order to create functional networks, the degradation process for 3D foams needs to be long

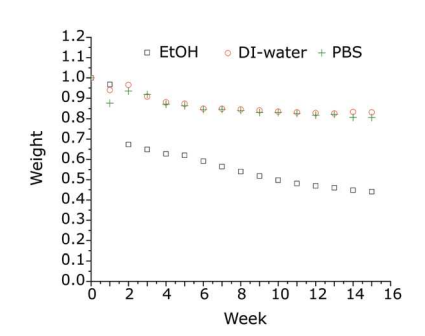


Fig. 6 Biodegradation plots (time vs. weight) of 6LCE foams in different media: ethanol (EtOH), deionized water, and PBS buffer.

enough to permit neurons to grow and differentiate into mature cellular phenotypes. Contrary to hydrogels, in which shape is not explicitly controlled, development of ECM in 3D polymeric scaffolds may require additional time to reach the particular shape. Thus, observing a long degradation time is encouraging for the use of the here reported LCE materials.

Experimental

Materials and methods

All air sensitive manipulations were carried out under nitrogen gas. ε-Caprolactone (ε-CL, from Alpha Aesar) was dried over calcium hydride and distilled under reduced pressure. D,L-Lactide was used as received (from Alpha Aesar). Dipentaerythritol, triethylamine, stannous 2-ethylhexanoate, chromium (vi) oxide, sodium sulfate, pyridinium chlorochromate, sodium azide, copper iodide, and sodium bicarbonate were used as received (Sigma-Aldrich). Sodium thiosulfate purchased from Fisher Scientific was used as received. 3-Chloroperbenzoic acid (m-CPBA, from Sigma-Aldrich) was dissolved in diethyl ether and this ether solution was washed with a buffer solution (prepared from 1.28 g sodium phosphate monobasic monohydrate and 8.24 g sodium phosphate dibasic heptahydrate in 800 mL distilled water at pH = 7.4). All solvents used for the synthesis and purification were EMD Millipore grade purified by a Pure-Solv solvent purification system (Innovative Technology Inc.). Dulbecco's modified Eagle medium (DMEM) with 4.5 g L⁻¹ glucose and sodium pyruvate without L-glutamine and Dulbecco's phosphate buffered saline (PBS) without calcium and magnesium were purchased from Corning CellGrO. Penicillin streptomycin solution (Pen-Strep) was purchased from Thermo Scientific. Fetal bovine serum (FBS) and trypsin were purchased from HyClone. Formaldehyde solution for molecular biology, 36.5-38% in H₂O, was purchased from SIGMA Life Science. 4',6-Diamidino-2-phenylindole (DAPI), and UltraPure Agarose were purchased from Invitrogen. Reagent Alcohol 200 proof ACS grade (denatured ethanol) was purchased from VWR. The neuroblastoma cell line (SH-SY5Y) was purchased from American Type Culture Collection. Salt crystals (NaCl) were purchased from BDH.

¹H and ¹³C NMR of copolymers and LCEs were recorded in CDCl₃ at room temperature on a Bruker DMX 400 MHz instrument and referenced internally to residual peaks at 7.26 (¹H). Fourier Transform Infrared Spectroscopy spectra were recorded using a Bruker Vector 33 spectrometer equipped with attenuated total reflection (ATR) mode.

Scanning electron microscopy (SEM) was performed on freeze fractured elastomer foams, gold coated (700 Å) using a sputter coater (Hummer VI-A, Anatech Ltd, VA) at 10 mA DC for 3 min. Images were acquired using a Hitachi S-2600N SEM.

Uniaxial compression experiments were performed on a TA Instruments Q800 dynamic mechanical analyzer (DMA) equipped with compression clamps. Experiments were conducted in controlled force mode under ambient conditions and the samples were compressed at a rate of 0.5 mm min⁻¹ until the compressive force limit was reached.

Polarized optical microscopy (POM) was performed using an Olympus BX53 polarizing microscope (20×) equipped with a Linkam LTS420 heating/cooling stage. All samples were initially heated to the isotropic liquid phase and then cooled to observe the temperature range at a rate of 0.1 °C min⁻¹.

Thermal phase transitions were determined using a Thermal Analysis Q100 Differential Scanning Calorimeter rate of 10 °C min⁻¹ from −80 °C to +170 °C under a N₂ atmosphere. Thermal degradation studies were carried out with a Hi-Res thermogravimetric analysis (TGA)-2950 thermal analyzer under a N_2 atmosphere with a ramp of 10 °C min⁻¹.

Small angle X-ray diffraction (SAXS) data were collected at beamline 7.3.3 of the Advanced Light Source (ALS) at Berkeley.

For cell culture, four equal pieces of elastomer were cut to a 2 mm width. Multiple techniques were utilized to sterilize the elastomers, including washing with 70% v/v ethanol, UV irradiation for 20 min, rinsing with sterile water, and rinsing with phosphatebuffered saline (PBS). Once the samples were ready for cell seeding, they were mixed with 1 wt% poly-D-lysine and washed with 2% agarose with DMEM substrate to further cell-to-cell adhesion, and prevent adhesion to the dish respectively. 1.5 \times 10⁴ cells were suspended in 100 mL of media and slowly placed onto the elastomer by the use of a pipet. The elastomers were then placed in a 5% CO₂ atmosphere humidity chamber at 37 °C. Every 48 hours, the media was changed and the elastomers were washed with 0.5 mL PBS. After 7, 14, and 30 days, the cells were fixed using 4% paraformaldehyde in PBS and stained with 0.1% DAPI (in PBS with 0.1% Triton-X) to be imaged with fluorescence confocal microscopy analysis. 3D images were created and analyzed.

Fluorescence confocal microscopy was carried out using an Olympus FV1000 equipped with three laser lines and Image³⁹ was used for image analysis/processing. Fluorescence for cell proliferation was measured using a Molecular Devices M4 SpectroMax Multi-Mode Microplate Reader. The porosity of the LCE scaffolds was determined from four times 1 mm scans through the LCE foams.

Porosity studies were also performed using a SkyScan 1172 Micro CT Scanner (Bruker). The X-ray source was set at a voltage of 60 kV and current of 167 μ A, with a power of 10 W. The foam samples as obtained had a quasi cylindrical shape and were mounted vertically on the sample holder and scanned at a resolution of 8 µm, with a step of 0.4 degrees for a total rotation angle of 180 degrees, and with 8 frames averaging per step. Cone-beam volumetric (Feldkamp algorithm) reconstruction was used. The obtained slices after the reconstruction contain information of the density of the foam expressed in 256 grey levels and with a unit image point (voxel) size of 8 µm. The images of the slices in bmp format were loaded into the morphology analysis software CTan (Bruker) and were processed to measure the porosity of the sample.

Conclusions

We here presented a biodegradable, porous SmA LCE foam showing a new morphology obtained using a salt-leaching method. This process permitted a better control over pore size

and pore size distribution within the LCE bulk. The mechanical properties very closely mimic neural environments, ideal to host brain cells. On-going degradation studies involving LCE foams with seeded cells are being made to compare hydrolytic degradation rates, shown here, to obtain both hydrolytic degradation by the media as well as enzymatic degradation. Tunable and appropriate degradation rates will be designed to complement temporal aspects of neuronal maturation. Using this approach, the scaffolds will support the spatial location of immature cells while degrading at a rate for unimpeded neurite formation in maturing cells, the latter being critical for intercellular communication. Thus, the presented LCE foam materials are capable of supporting in vitro longitudinal neuronal growth in many layers and spatial orientations to create functional neural networks reminiscent of endogenous tissue.

Authors' contributions

M. E. P., and E. H. drafted the article with significant contributions from L. T. J. K., E. J. F., J. A. M. and R. J. C. M. E. P. performed most synthesis, characterization, and testing of materials, H. A., B. K., and S. T. R. assisted with the synthesis of key intermediates, helped with characterization. S. U. performed all cell culture, and staining under the supervision and guidance of E. J. F., J. A. M. and R. J. C. S. U., and M. E. P., performed all confocal fluorescence microscopy studies, with the supervision and guidance of R. J. C. M. E. P., M. T. B., and S. L. M. did all mechanical testing with the supervision and guidance of L. T. J. K. M. E. P. and Z. K. performed the Micro CT measurements for porosity studies. The authors would also like to acknowledge the Surface and Optical Analysis Facility at the National Polymer Innovation Center for the Micro CT imaging and morphology analysis.

Conflicts of interest

The authors have no competing financial interests to declare.

Acknowledgements

The authors would like to thank the National Science Foundation for funding the NSF-REU Program (CHE-1659571) and Kent State University for financial support of a collaborative research grant and the Regenerative Medicine Initiative at Kent State (ReMedIKS). The authors are also thankful to Dr E. Schaible for help with SAXS measurements at the Advanced Light Source, Berkeley. Beamline 7.3.3 of the Advanced Light Source is supported by the Director of the Office of Science, Office of Basic Energy Sciences, of the U.S. Department of Energy under Contract No. DE-AC02-05CH11231. The authors would also like to thank the Materials Characterization facility at Liquid Crystal Institute (LCI), where current SEM images were obtained. M. P. and E. H. would like to thank Dr Michel Mitov (CNRS) for the motivating discussions on LCEs and pointing out O. Lehmann's

article published in 1909 detailing the very first suggestion of artificial muscle-motors using LCs.

References

- 1 O. Lehmann, J. Phys. Theor. Appl., 1909, 8, 713-735.
- 2 P.-G. deGennes, C. R. Acad. Sci., Ser. IIb: Mec., Phys., Chim., Astron., 1997, 324, 343-348.
- 3 M.-H. Li and P. Keller, Philos. Trans. R. Soc., A, 2006, 364, 2763-2777.
- 4 A. Sanchez-Ferrer, T. Fischl, M. Stubenrauch, A. Albrecht, H. Wurmus, M. Hoffmann and H. Finkelmann, Adv. Mater., 2011, 23, 4526-4530.
- 5 A. Agrawal, H. Y. Chen, H. Kim, B. H. Zhu, O. Adetiba, A. Miranda, A. C. Chipara, P. M. Ajayan, J. G. Jacot and R. Verduzco, ACS Macro Lett., 2016, 5, 1386-1390.
- 6 E. Aurand, J. Wagner, C. Lanning and K. Bjugstad, J. Funct. Biomater., 2012, 3, 839.
- 7 U. Novak and A. H. Kaye, *J. Clin. Neurosci.*, 2000, 7, 280–290.
- 8 D. F. Williams, Biomaterials, 2008, 29, 2941-2953.
- 9 Y. Martin and P. Vermette, *Biomaterials*, 2005, 26, 7481–7503.
- 10 J. E. Scott, J. Anat., 1995, 187, 259-269.
- 11 F. Rosso, A. Giordano, M. Barbarisi and A. Barbarisi, J. Cell. Physiol., 2004, 199, 174-180.
- 12 S. F. Badylak, Biomaterials, 2007, 28, 3587-3593.
- 13 H. Cheng, P. S. Hill, D. J. Siegwart, N. Vacanti, A. K. R. Lytton-Jean, S. W. Cho, A. Ye, R. Langer and D. G. Anderson, Adv. Mater., 2011, 23, H95-H100.
- 14 E. M. Ahmed, J. Adv. Res., 2015, 6, 105-121.
- 15 K. J. R. Lewis and K. S. Anseth, MRS Bull., 2013, 38, 260–268.
- 16 D. L. Alge, M. A. Azagarsamy, D. F. Donohue and K. S. Anseth, Biomacromolecules, 2013, 14, 949-953.
- 17 J. D. McCall, J. E. Luoma and K. S. Anseth, Drug Delivery Transl. Res., 2012, 2, 305-312.
- 18 C. A. DeForest and K. S. Anseth, Annu. Rev. Chem. Biomol. Eng., 2012, 3, 421-444.
- 19 B. V. Slaughter, S. S. Khurshid, O. Z. Fisher, A. Khademhosseini and N. A. Peppas, Adv. Mater., 2009, 21, 3307-3329.
- 20 J. Zhong, A. Chan, L. Morad, H. I. Kornblum, G. P. Fan and S. T. Carmichael, Neurorehabil Neural Repair, 2010, 24, 636-644.
- 21 O. Qutachi, J. R. Vetsch, D. Gill, H. Cox, D. J. Scurr, S. Hofmann, R. Muller, R. A. Quirk, K. M. ShakeSheff and C. V. Rahman, Acta Biomater., 2014, 10, 5090-5098.
- 22 C. Berkland, K. Kim and D. W. Pack, Pharm. Res., 2003, 20, 1055-1062.

- 23 L. A. Smith, X. H. Liu and P. X. Ma, Soft Matter, 2008, 4, 2144-2149.
- 24 M. P. Lutolf and J. A. Hubbell, Nat. Biotechnol., 2005, 23, 47-55.
- 25 Q. P. Hou, D. W. Grijpma and J. Feijen, Biomaterials, 2003, 24, 1937-1947.
- 26 R. T. Tran, E. Naseri, A. Kolasnikov, X. C. Bai and J. Yang, Biotechnol. Appl. Biochem., 2011, 58, 335-344.
- 27 B. Dhandayuthapani, Y. Yoshida, T. Maekawa and D. S. Kumar, Int. J. Polym. Sci., 2011, 2011, 1.
- 28 P. A. Janmey and R. T. Miller, J. Cell Sci., 2011, 124, 9-18.
- 29 A. Sharma, A. Neshat, C. J. Mahnen, A. D. Nielsen, J. Snyder, T. L. Stankovich, B. G. Daum, E. M. LaSpina, G. Beltrano, Y. Gao, S. Li, B.-W. Park, R. J. Clements, E. J. Freeman, C. Malcuit, J. A. McDonough, L. T. J. Korley, T. Hegmann and E. Hegmann, Macromol. Biosci., 2015, 15, 200-214.
- 30 A. Sharma, T. Mori, C. J. Mahnen, H. R. Everson, M. T. Leslie, A. D. Nielsen, L. Lussier, C. Zhu, C. Malcuit, T. Hegmann, J. A. McDonough, E. J. Freeman, L. T. J. Korley, R. J. Clements and E. Hegmann, Macromolecular Bioscience, 2017, 17, 1600278.
- 31 Y. X. Gao, T. Mori, S. Manning, Y. Zhao, A. D. Nielsen, A. Neshat, A. Sharma, C. J. Mahnen, H. R. Everson, S. Crotty, R. J. Clements, C. Malcuit and E. Hegmann, ACS Macro Lett., 2016, 5, 14-19.
- 32 M. E. Prevot, S. Ustunel, L. E. Bergquist, R. Cukeli, Y. X. Gao, T. Mori, L. Pauline, R. J. Clements and E. Hegmann, J. Visualized Exp., 2017, 11, DOI: 10.3791/55452.
- 33 J. Dey, H. Xu, J. H. Shen, P. Thevenot, S. R. Gondi, K. T. Nguyen, B. S. Sumerlin, L. P. Tang and J. Yang, Biomaterials, 2008, 29, 4637-4649.
- 34 J. I. Forster, S. Koglsberger, C. Trefois, O. Boyd, A. S. Baumuratov, L. Buck, R. Balling and P. M. A. Antony, J. Biomol. Screening, 2016, 21, 496-509.
- 35 J. Rouwkema, N. C. Rivron and C. A. van Blitterswijk, Trends Biotechnol., 2008, 26, 434-441.
- 36 C. T. McKee, J. A. Last, P. Russell and C. J. Murphy, Tissue Eng., Part B, 2011, 17, 155-164.
- 37 M. E. Prévôt and E. Hegmann, ACS Books, Books: Advances in Bioinspired and Biomedical Materials, ACS 1253, 2017, ch. 1, vol. 2, pp. 3-45, DOI: 10.1021/bk-2017-1253.ch001.
- 38 S. W. Desouza and J. Dobbing, Exp. Neurol., 1971, 32, 431-439.
- 39 C. A. Schneider, W. S. Rasband and K. W. Eliceiri, Nat. Methods, 2012, 9, 671-675.